Murdocca *et al. Human Genomics* (2025) 19:131
https://doi.org/10.1186/s40246-025-00848-0

Human Genomics

RESEARCH Open Access

Structural and functional impact of the POLD1 Ser605del variant in MDPL syndrome: insights from protein–protein interactions

Michela Murdocca[1†], Isabella Romeo[2,3†], Serena Maccaroni[1], Antonio Curcio[2], Gerardo Pepe[4], Manuela Helmer-Citterich[4], Stefano Alcaro[2,3], Giuseppe Novelli[1] and Federica Sangiuolo[1*]

Abstract

Background Mandibular hypoplasia, Deafness, Progeroid features, and Lipodystrophy (MDPL) syndrome is a very rare genetic disorder linked to variants in the *POLD1* gene, which encodes the catalytic subunit of DNA polymerase delta, a key enzyme involved in DNA replication and repair. Most patients carry a recurrent in frame deletion (p.Ser605del) within the active site of the p125 subunit. Despite its rarity, understanding the functional consequences of the Ser605del variant has broad implications for aging-related diseases and genome stability.

Methods We combined structural modelling, molecular dynamics simulations, and protein–protein interaction (PPIs) analyses to evaluate the impact of Ser605del in the catalytic activity of DNA polymerase delta. Bioinformatic tools were applied to characterize its interaction network. RT-q PCR and Western Blot were performed to assess expression levels of POLD1, TRF1, and PARP1 in human dermal fibroblasts (HDFs) of three MDPL patients of different ages. Cells were monitored at different passages, both in basal condition and after damage by X irradiation. POLD1/TRF1 interaction was confirmed by immunoprecipitation analyses.

Results Using molecular docking, molecular dynamics simulations and thermodynamic analyses, we found that Ser605del affects the DNA-binding site, impairing dTTP binding. The deletion alters short linear motifs involved in protein–protein interactions (PPIs), allowing the acquisition of a F/Y-X-L-X-P (FSLYP) consensus sequence with TRF1, a telomeric protein. In silico analyses highlighted a stronger interaction between the Ser605del POLD1 variant and TRF1. Experiments on MDPL fibroblasts confirmed a stronger POLD1–TRF1 binding and revealed dysregulation of PARP1, involved in telomere maintenance. Following X-ray irradiation, aimed at exacerbating the cellular phenotype, we observed a decreasing trend in these markers, which reached statistical significance particularly in one older patient.

Conclusions We identified a novel short linear motif (FSLYP) in the Ser605del POLD1 protein that mediates abnormal interaction with TRF1, revealing a structural and functional link between POLD1 and telomere biology, contributing

[†]Michela Murdocca and Isabella Romeo have contributed equally to this work.

*Correspondence:
Federica Sangiuolo
sangiuolo@med.uniroma2.it

Full list of author information is available at the end of the article

© The Author(s) 2025. **Open Access** This article is licensed under a Creative Commons Attribution-NonCommercial-NoDerivatives 4.0 International License, which permits any non-commercial use, sharing, distribution and reproduction in any medium or format, as long as you give appropriate credit to the original author(s) and the source, provide a link to the Creative Commons licence, and indicate if you modified the licensed material. You do not have permission under this licence to share adapted material derived from this article or parts of it. The images or other third party material in this article are included in the article's Creative Commons licence, unless indicated otherwise in a credit line to the material. If material is not included in the article's Creative Commons licence and your intended use is not permitted by statutory regulation or exceeds the permitted use, you will need to obtain permission directly from the copyright holder. To view a copy of this licence, visit http://creativecommons.org/licenses/by-nc-nd/4.0/.

to premature aging phenotypes. This work provides new insights into MDPL pathogenesis and lays the foundation for future research into aging-related therapies.

Keywords MDPL syndrome, POLD1, DNA damage, TRF1, Rare Disease, Immunoprecipitation, Protein-Protein Interaction, Molecular Dynamic Simulation, Structural modeling

Introduction

A genetic disease is not just a consequence of a pathogenic mutation in a single gene, but instead considers the interplay of multiple molecular processes.

The links among these processes are inserted in the interactome, a network that integrates all physical synergies within a cell, such as protein-protein, regulatory protein–DNA and metabolic interactions [1]. Thus, clarifying the clinical pathogenic outcomes of a genetic variant is essential for the advancement of precision medicine.

Despite advancements in human genome sequencing, our ability to fully understand the functional and biological implications of identified genetic variants remains limited. Several key issues in the field are still unresolved, including the phenotypic effects of different mutations within the same gene and the mechanisms by which a single pathogenic variant may affect different cell types.

Given the limited availability of experimental data for many rare diseases, computational protocols have become essential tools for predicting the molecular impact of pathogenic variants on protein stability, dynamics, and protein-protein interactions. While most research has concentrated on the intramolecular effects of mutations, there is growing recognition of the crucial role played by the mutations in the assembly of proteins into complexes.

Indeed, although proteomic techniques have clarified the subunit composition of many complexes, their three-dimensional structure is often essential for understanding their mechanisms. High-resolution structural studies of heteromeric complexes are particularly challenging due to their large size, difficulties in obtaining homogeneous samples and to the limitations of co-expression and recombinant systems, which hinder their analysis through X-ray crystallography and NMR (Nuclear Magnetic Resonance). However, recent advances in co-expression systems, purification from native sources, and cryo-electron microscopy have revolutionized the structural characterization of these complexes.

In the context of very rare diseases, we have specifically focused our attention on DNA polymerase delta (Pol δ), and particularly on its catalytic subunit encoded by *POLD1* gene. Pol δ is responsible for lagging-strand DNA synthesis during DNA replication [2]. It is a four-subunit enzyme, whose activity could be reconstituted in vitro [3] and whose cryo-EM structure has recently been determined [4].

Specifically, the protein product of the *POLD1* gene is the p125 catalytic subunit of Pol δ, which interacts, forming a heterotetramer with three smaller subunits encoded by the *POLD3* (p66), *POLD2* (p50), and *POLD4* (p12) genes [5]. p50 acts as a scaffold, interacting with all other subunits [6]. The most common pathogenic variant occurring in *POLD1* gene is a heterozygous *in frame* single-codon deletion (named c.1812_1814del: p.Ser605del) that abolishes DNA polymerase activity but only mildly impairs 3'- to 5'-exonuclease activity. This variant causes the MDPL syndrome (Mandibular hypoplasia, Deafness, and Progeroid features with concomitant Lipodystrophy; MIM #615381), a distinct progeroid multisystemic disorder characterized by subcutaneous lipodystrophy, deafness, mandibular hypoplasia and hypogonadism in males.

To date, ~ 40 patients have been reported worldwide to be affected by MDPL with about 70% from Europe and the Americas and about 30% from Asia; however, the pathogenetic mechanism of the disease remains unclear [7].

The Ser605del variant occurs within motif A, representing an 11-amino-acid highly conserved region of the Pol δ catalytic subunit. This region plays a critical role in aligning the incoming complementary deoxynucleotide (dNTP) with the primer terminus, as well as in coordinating and catalysing the formation of phosphodiester bonds. Weedon et al. have hypothesized that a defective p125 subunit may lead to an increased incidence of stalled replication forks, thereby increasing genomic instability, triggering cell cycle checkpoint responses, and enhancing cell senescence and death [8]. By a structural point of view, the Ser605del disrupts the polymerase active site, showing a complete loss of polymerase activity and a weakly reduced exonuclease capacity. Thus, the mutant protein retains the ability to bind DNA, but it is unable to catalyse polymerization.

In this study, we investigated how Ser605del variant affects the DNA binding site of p125 subunit. Specifically, using a combination of molecular docking, molecular dynamics (MD) simulations, and binding free energy calculations, we aim to assess the impact of the deletion on the protein's structural stability and its ability to bind the incoming nucleotide dTTP during DNA synthesis. Successively, to explore additional functional consequences, we also analyse whether the deletion alters short linear motifs (SLiMs) involved in protein–protein interactions (PPIs). These motifs mediate transient yet specific interactions, and their loss or gain can significantly affect

cellular function. Sequence analysis of the Ser605-deleted p125 protein revealed the presence of a F/Y-X-L-X-P functional motif (FSLYP), which is absent in the wild-type sequence. This motif is known to mediate interactions with the TRFH domain of Telomere Repeat Binding Factor 1 (TRF1), suggesting that the Ser605 deletion may confer a novel TRF1-binding potential to p125.

Strikingly, TRF1 is a component of the shelterin complex at telomeres, essential for maintaining their functional integrity. It facilitates DNA replication and plays a key role in protecting telomeres by limiting DNA damage induced by subtelomeric recombination, as well as safeguarding short telomeres from inappropriate recombination [9]. Considering the previously described telomere shortening in MDPL human dermal fibroblasts (HDFs),[10,11] a possible role of this protein in the disease pathogenesis is intriguing. This finding prompted a computational analysis to explore the interaction between TRF1 and both WT and deleted p125, respectively.

Our analysis, combining protein–protein docking, binding pocket profiling and MD simulations, suggests that the Ser605del variant of p125 exhibits a favourable binding interface with TRF1, potentially resulting in a more stable interaction compared to the wild-type protein.

Through an integrated approach, we evaluated these aspects in vitro using HDFs of three MDPL patients of different ages, and at different passages (p13 and p20) to reproduce the aging process. Cells were monitored both in their basal condition and after damage by X-ray irradiation, for triggering any possible protein repair activity, as already reported in our previous work [10].

Thus, we first assessed the expression levels of p125 and TRF1 proteins, and then, by immunoprecipitation analysis, their interaction, which was found to be stronger in cells carrying the Ser605del variant at the basal level. Due to the striking link between TRF1 and PARP1, we analyzed the expression of this telomere-associated protein in our cells, assessing dysregulation at both the transcript and protein levels in MDPL cells.

In this study, the experimental validation of computational predictions enabled us to explore the effects of the Ser605del mutation on protein–protein interactions, revealing novel insights that may contribute to the development of future therapeutic strategies for aging-related diseases.

Methods

Protein and ligand preparation

Based on the availability of structural data in the PDB and the corresponding resolution, we meticulously selected and downloaded the three-dimensional (3D) coordinates of POLD1, included in the human polymerase delta holoenzyme (PDB ID: 6TNY) and TRF1, encompassing the TRFH domain and the TIN2 peptide complex (PDB ID: 3BQO). Starting from the WT POLD1 structure, the mutant variant was generated by deleting Ser605 and adjusting the distance between Ser604 and Leu606 to 1.32 Å, corresponding to the average peptide bond length, using the Maestro graphical user interface. Subsequently, these structures were processed and subjected to energy optimization using the Protein Preparation Wizard v4.1 (Schrödinger Release 2020-4: Schrödinger, LLC, New York, NY, 2020), implemented in Maestro v4.1, with OPLS_2005 force field [12]. Particularly, residual crystallographic buffer components and water molecules were removed, hydrogen atoms were incorporated, and the protonation states of side chains were assigned at physiological pH. dTTP was prepared using the LigPrep Tool v4.5 (Schrödinger Release 2020-4: Schrödinger, LLC, New York, NY, 2020). This process involved the addition of hydrogen atoms and calculating ionization states through Epik at pH 7.4. Each structure underwent the default energy minimization steps of LigPrep using the OPLS_2005 force field. The total charge of dTTP at physiological pH was evaluated using the MSketch tool v16.3.28, which identified two predominant charge states: one carrying three negative charges (51.03%) and another with four negative charges (48.69%).

Docking and molecular dynamics (MD) simulations

The two predominant dTTP species were subjected to molecular docking simulations using the Glide SP protocol v7.8 [13] (Schrödinger Release 2020-4: Glide, Schrödinger, LLC, New York, NY, 2020) on both WT and mutant POLD1. Glide grids were generated using the Receptor Grid Generation tool, with the grid centered on Ser604 in both the WT and mutant structures, defining an inner box of $10 \times 10 \times 10$ Å and ten ligand poses were generated.

Subsequently, the complexes between the predominant dTTP macrospecies and both WT and mutant POLD1 were subjected to 100 ns of MDs using Desmond v4.4 [14] (Schrödinger Release 2020-4: Desmond Molecular Dynamics System, D. E. Shaw Research, New York, NY, 2020), with the OPLS_2005 force field. The complexes were placed in an orthorhombic simulation box with a 10 Å buffer of TIP4P water [15], adding counterions to neutralize the net system charge. Following solvation, the systems underwent energy minimization and equilibration using the Martyna–Tobias–Klein (MTK_NPT) isothermal–isobaric ensemble. Equilibration was performed under NVT and NPT conditions at a pressure of 1 atm, reaching a temperature of 300 K using the Berendsen thermostat–barostat. Trajectory frames were collected every 100 ps and analyzed using the Simulation Interaction Diagram (SID) to investigate the obtained trajectories, in terms of geometrical parameters and interactions.

Finally, the MM-GBSA (Molecular Mechanics–Generalized Born Surface Area) analysis was conducted [16] at a frequency of one every 10 frames, employing molecular mechanics and continuum solvation models to determine the binding free energies (ΔGbind).

Volume calculation and protein–protein interaction

To analyze the binding site and cavity found between L656–L674 and V768–V782 helices, we used the SiteMap program in Maestro [17]. This algorithm identifies protein surface regions suitable for ligand binding, offering insights into hydrophobic and hydrophilic characteristics. Additionally, SiteMap enables the calculation of cavity volume within a specified pocket, allowing for a comparative analysis of volumetric differences between WT and mutant p125.

The subsequent protein-protein docking of p125 and TRF1 was conducted using the HADDOCK 2.4 (High Ambiguity-Driven Biomolecular Docking) web server [18]. This approach integrates Coulomb electrostatic interactions, non-bonded intermolecular Van der Waals forces, empirically derived desolvation energies, and buried surface area calculations. For p125, the amino acids F603, L606, and P608, located within the F/Y-X-L-X-P motif, were designated as active residues in both the WT and mutant forms, while passive residues were automatically chosen as those surrounding the active residues before docking. Regarding TRF1, the residues at positions 86, 102, 106, 109, 115, 120, 123, 124, 127, 130, 131, 139, 142, 147, and 192, which are involved in the TRF1TRFH–TIN2TBM interaction, were selected as active residues, with passive residues automatically assigned [19]. For each complex, the docking procedure employed the following sampling parameters: 1000 structures for rigid-body docking, 200 for final refinement, and a cut-off distance of 5.0 Å to define neighboring flexible regions. For each complex, the docked structures were subsequently imported into the Maestro interface of the Schrödinger Suite 2024-2 in PDB format for visual inspection.

To validate the docking protocol, a re-docking of the TRFH domain of TRF1 with the TIN2 peptide was performed, using the previously defined TRFH active residues and considering all TIN2 residues as active. Structural alignment of the resulting model produced an alignment score of 0.01 and a backbone RMSD of 0.62 Å, confirming the reliability of the docking protocol.

The visualization of 3D structures and the generation of images were performed using the Maestro graphical interface and Chimera software [20].

GRID-based pharmacophore model (GBPM)

For both the WT p125/TRF1 and mutant p125/TRF1 complexes, all simulation frames were included in the GBPM analysis [21]. To identify key hydrophobic regions and hydrogen bond donor and acceptor sites, the DRY, N1, and O GRID probes were employed, respectively. In this context, TRF1 was designated as the guest, while both WT and mutant POLD1 served as hosts. Residues at the protein-protein interface were selected based on their proximity (within 3 Å) to the most energetically relevant points (GBPM features) identified in the computed molecular interaction fields (MIFs). A threshold of 30% above the global minimum energy was applied to filter significant interaction regions. The resulting interaction hotspots were determined by summing the interaction energies associated with the relevant GBPM features. This protocol follows a previously established and reported methodology [22].

Motif analysis

To investigate the impact of the Ser605 deletion on the linear motifs present in p125, we compared the WT and mutant sequences using two motif prediction tools: ELM (Eukaryotic Linear Motifs, http://elm.eu.org) and PROSITE (https://prosite.expasy.org). The amino acid sequences of the WT [Uniprot ID: P28340] and mutant p125 were input into both platforms to identify potential gains or losses of functional motifs associated with PPI, post-translational modifications, or cellular localization. Additionally, phosphorylation sites around the Ser605 region were analyzed using ELM, which allowed the identification of phosphorylation recognition motifs and potential changes in post-translational regulation.

Cell cultures

Three MDPL patients of different ages were selected: BRY (8 years old, XY), PX (14 years old, XX), and LRX (21 years old, XX). Analyses were conducted by comparing patients to age-matched healthy controls: the youngest patient, BRY, was compared to WT1 (5 years old, XY), while the older patients, PX and LRX, were compared to WT2 (15 years old, XX). Human dermal fibroblasts was obtained starting from skin punch biopsy and cultured in DMEM High Glucose (Gibco, Thermo Fisher Scientific, USA) media, containing 10% FBS (Gibco, Thermo Fisher Scientific, USA), 1% L-Glutamine (PAA, The Cell Culture Company, Germany), 1% Penicillin/Streptomycin (PAA, The Cell Culture Company, Germany), 1% NEAA (Gibco, Thermo Fisher Scientific, USA) and 0.1% β-mercaptoethanol (Gibco, Thermo Fisher Scientific, USA).

For X-irradiation (1 Gy ray), HDFs were cultured under standard conditions as previously described [10]. Once the cells reached the appropriate confluence, they were either exposed to 1 Gy of ionizing radiation, then they were collected and analysed 24 h (+24 h) after irradiation.

Gene expression analyses

Total RNA was extracted by cells using TRIzol Reagent (Invitrogen, Life Technologies Corporation, Carlsbad, CA, USA), according to the manufacturer's instructions, followed by DNase I (RNase-free) treatment (Ambion, Life Technologies Corporation, Foster City, CA, USA). One microgram of RNA was reverse transcribed using the High-Capacity cDNA Archive Kit (Life Technologies Corporation, Foster City, CA, USA) and subsequently used for RT-qPCR analysis. mRNA levels were quantified using SYBR Green chemistry (Life Technologies Corporation, Foster City, CA, USA), with GAPDH serving as the reference gene. Primer sequences are available upon request. Relative gene expression was calculated using the $2^{-\Delta Ct}$ and comparative ΔΔCt methods.

Western blotting

HDFs were grown in T25 flasks and collected with 0.05% trypsin-EDTA (0.05% Trypsin, 0.53 mM EDTA, 1X; Corning) when they reached 75% confluence. They were rinsed with ice-cold DPBS (Dulbecco's Phospate-Buffered Saline without calcium &magnesium, Corning, REF 21-031-CV) twice, harvested by centrifugation and lysed in RIPA-Buffer (PierceTM RIPA Buffer, REF 89901,) adding freshly a cocktail of protease inhibitors (HaltTM Protease Inhibitor Cocktail 100X, Prod. #1862209, Thermo fisher Scientific). After incubated 30 min on ice, samples were centrifuged at 14,000 g, at 4 °C, for 20 min. The supernatants were prepared for Western blot by adding LDS Sample buffer (B0007, Thermo Fisher Scientific) and sample reducing agent (B0009, Thermo Fisher Scientific). The protein extracts were denatured at 95° for 10 min. Proteins were separated by 4–12% SDS-PAGE gel (NW04125BOX, Thermo Fisher Scientific), then nitrocellulose membranes (88018, Thermo Fisher Scientific) were probed with primary antibodies. The primary antibodies used are: anti-POLD1 antibody (diluted 1:500, ab225907, Abcam), TRF1 (1:1000, ab1423, Abcam) and the loading control GAPDH (diluted 1:2000, REF MA5-15738, Thermo Fisher Scientific). Horseradish peroxidase-conjugated secondary antibodies were used: Goat anti-Rabbit (diluted 1:1000, REF 32460, Thermo Fisher Scientific), Goat anti-mouse (diluted 1:10000, REF 31430, Thermo Fisher Scientific). Proteins were visualized with ECL (RPN2235, Cytiva), chemiluminescence signals were detected using the ChemiDocTM Imaging System (Bio-rad) and densitometric analyses was performed by Image Lab software.

For DNA damage induction, cells were growth in the same conditions and irradiated by 1 Gy X-irradiation when they reached 75% confluence and harvested 24 h later.

Immunoprecipitation

For immunoprecipitations, proteins were extracted as previously described. 30 ug of the total protein extract were kept as input, while 1 mg was used for immunoprecipitation. Cellular extracts were incubated for 1 h at 4 °C with 30 µL of magnetic beads (Dynabeads™ Protein G, 10003D). The protein extract was then incubated with 5 µg of primary antibody overnight at 4 °C. For POLD1 and TRF1 immunoprecipitation, the following primary antibodies were used: anti-POLD1 antibody (1:500 dilution, ab225907, Abcam) and anti-TRF1 antibody (ab1423, Abcam). An equal amount of protein extract was incubated with normal rabbit IgG (Santa Cruz, sc-2027) as a negative control ("Neg"). The following day, the protein extract was incubated with 30 µL of magnetic beads for 1 h at 4 °C. The supernatant was then removed, and the beads were washed twice with RIPA buffer and once with PBS. Proteins were denatured by adding 2X LDS Sample Buffer (B0007, Thermo Fisher Scientific) and Sample Reducing Agent (B0009, Thermo Fisher Scientific), followed by boiling at 95 °C for 10 min. Magnetic beads were removed, and the proteins were analyzed by western blotting and the detection was made as previously described.

Statistical analyses

For the in vitro experiment statistical analysis was carried out using GraphPad Prism 10 software. The differences between groups were tested by t-test and one-way ANOVA test. Values provided in the figures are means of three independent experiments ± standard error of the mean (SEM). The level of significance was established at $^{*}p < 0.05$, $^{**}p < 0.01$, $^{***}p < 0.001$, $^{****}p < 0.0001$.

Results

Effect of Ser605del on p125 structure

First of all, we investigated the impact of the Ser605del on structural stability and DNA synthesis processivity of p125, respect to wild type one (WT). To achieve this, we first selected a high-resolution cryo-EM model of p125. Specifically, we used the model of the human polymerase with Protein Data Bank (PDB) ID 6TNY [5], from which the structure was extracted. Starting from the WT model, we generated the mutant by deleting Ser605, and both structures were properly prepared and subjected to energy minimization (Fig. 1A). To further validate the mutated model, we employed AlphaFold [23] to predict the mutant p125. The predicted model showed a ranking confidence score of 0.91, suggesting high reliability. Importantly, the predicted and generated structures exhibited a high degree of similarity, with a backbone RMSD equal to 1.06 Å across aligned residues, indicating that both models adopt comparable global conformations, above all close to the active site residues (See Figure

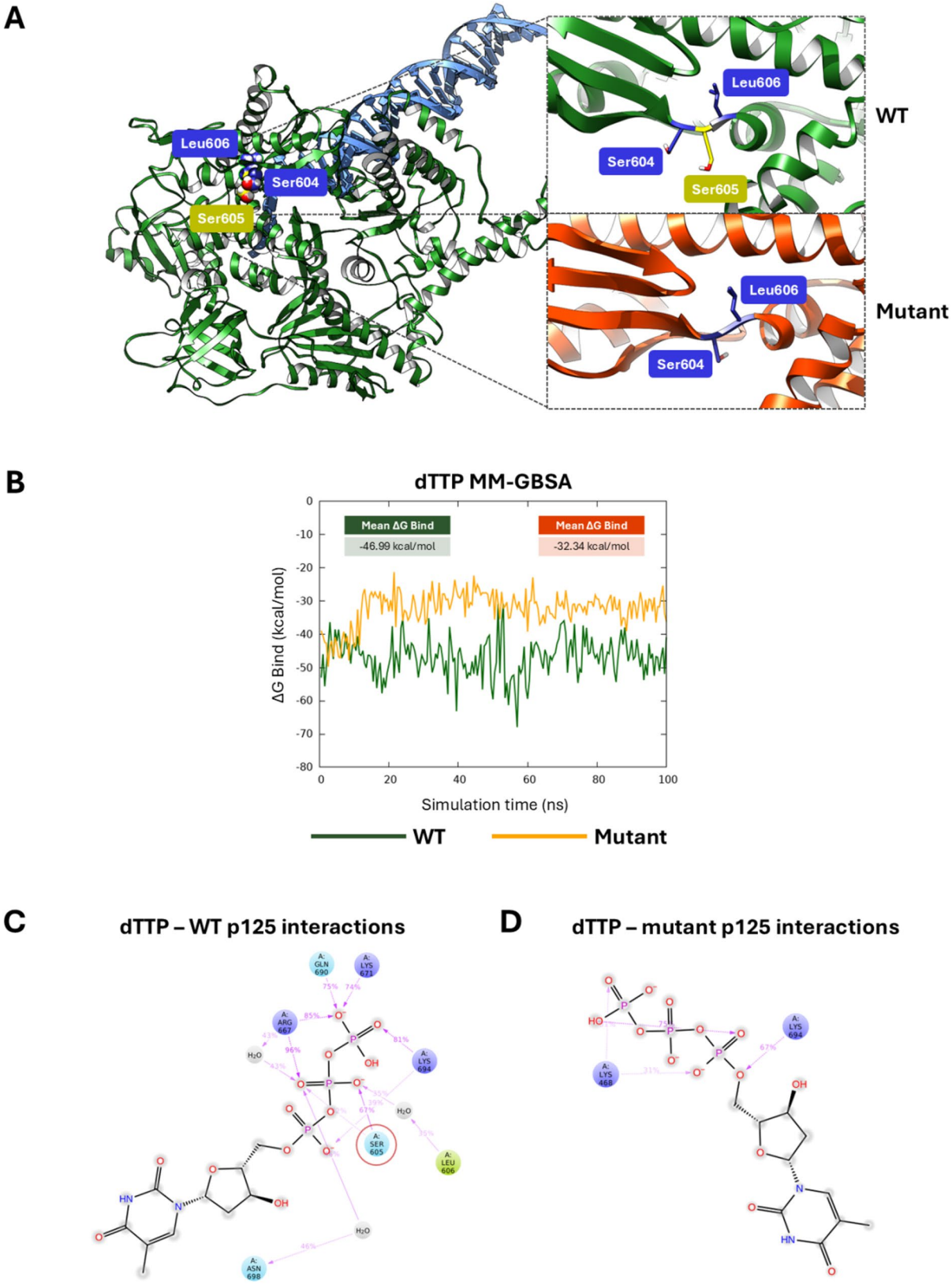

Fig. 1 Molecular dynamics insights into p125–dTTP interactions in WT and mutant forms. **A** 3D structures of p125 in its wild-type form (shown in green) and mutant form (shown in orange). Residues Ser604 and Leu606 are highlighted in blue, while the deleted Ser605 residue is marked in yellow; **B** MM-GBSA free energy analysis of dTTP binding in complex with WT and mutant p125; **C** and **D** Images showing dTTP-p125$_{WT}$ (**C**) and dTTP-p125$_{Mutant}$ (**D**) interactions, expressed as percentages over the MD simulation

S1). At this point, we performed the molecular docking simulation of the substrate, specifically the incoming nucleotide 2'-deoxythymidine triphosphate (dTTP), in both the WT and mutated protein, using Glide SP protocol v7.8. The total charge of dTTP was evaluated at physiological pH, revealing two predominant species.

The Glide Score (G-Score) values, calculated for both generated species, were consistently better for the WT protein than the mutant (See Figure S2). Furthermore, the predominant species exhibited a stronger theoretical binding affinity in the WT (-7.80 kcal/mol) compared to the mutant form (-5.99 kcal/mol), leading to the loss of a hydrogen bond (H-bond) with Ser605. To further explore theoretically how the mutation impacts the processivity of p125, we conducted 100 ns of molecular dynamics simulations (MDs) of the dTTP in complex with both the WT and mutant p125. Throughout the simulations, dTTP exhibited greater stability when bound to WT protein, as evidenced by lower root-mean-square deviation (RMSD) values calculated on the heavy atoms (See Figure S3). Meanwhile, the mutated structure showed a lower stability than WT, as resulted by the higher RMSD values. From a thermodynamic perspective, MM/GBSA free energy analysis revealed that dTTP demonstrated more favourable binding to WT p125 than the mutant form, as reflected by a lower ΔG_{Bind} trend (Fig. 1B). Specifically, the WT p125 exhibited a ΔG_{bind} of − 46.99 kcal/mol, whereas the mutant p125 showed a significantly less favorable value of − 32.34 kcal/mol. This difference of approximately 15 kcal/mol indicates a marked reduction in the stability and affinity of dTTP binding in the mutant form, further supporting the notion that the S605 deletion compromises the structural integrity of the active site and weakens nucleotide binding. Indeed, in the WT complex, the interaction between dTTP and Ser605 was preserved for 67% of the simulation run, whereas in the mutant structure, the interaction was completely abolished. Moreover, MDs revealed that in the WT, dTTP engaged additional stabilizing interactions, including hydrogen bonds with Arg667, Lys671, Gln690, and Lys694, as well as two water-bridges with Leu606 and Asn698. In contrast, in the mutant p125, only two hydrogen bonds were detected between dTTP and Lys468 and Lys694 residues (Fig. 1C and D).

Identification of slims in Ser605del p125 and potential interaction changes

Comparing wild type and mutated protein sequence of p125 binding site around Ser605, we observed that Ser605del generates a motif characterized by FSLYP sequence (Fig. 2A). To better contextualize the FSLYP motif emerging upon Ser605 deletion, we generated a sequence logo based on a curated set of known TRFH-binding sequences containing the F/Y-X-L-X-P consensus. The y-axis of the logo represents the information content at each position, indicating how conserved (i.e., informative) a residue is; the maximum value is approximately 4.32 bits ($\log_2(20)$), which corresponds to full conservation of a single amino acid.

The resulting logo highlights the positional enrichment of phenylalanine or tyrosine at position 1, leucine at position 3, and proline at position 5, features that mirror the FSLYP motif observed in our mutated sequence context (Fig. 2B). At this point, we utilized the ELM (Eukaryotic Linear Motif) database and PROSITE to identify and analyze SLiMs involved in protein-protein interactions (PPI) in both WT and mutant p125. Given the presence of the mutation, ELM facilitated the prediction of potential alterations in motif acquisition, which could affect binding affinities and functional interactions. Indeed, motif analysis identified the acquisition of the LIG_TRFH_1 linear motif in mutant p125, which is absent in the WT one (Fig. 2C). Since this motif has been identified in the mutated p125 and is known to mediate interactions with the TRFH domain of TRF1, it is plausible that the Ser605 deletion introduces a novel binding capability.

This could potentially enable p125 to interact with TRF1, a key component of the shelterin complex, which is essential for maintaining telomere integrity. It facilitates proper DNA replication and prevents damage arising from subtelomeric recombination. In addition to motif analysis, the phosphorylation site around the Ser605 region were evaluated. While no unique phosphorylation sites were identified in the mutant compared to the WT, motifs associated with GSK3-mediated phosphorylation, which is typically linked to protein inactivation, were consistently detected in both forms. These findings suggest that although the Ser605del affects motif acquisition and interaction potential, it does not appear to significantly alter phosphorylation-mediated regulatory mechanisms.

Transcript and protein expression levels of TRF1 and POLD1/p125 in MDPL and WT HDFs at p13 and p20

To investigate the impact of the Ser605del variant on *POLD1* gene and POLD1/p125 protein, we performed RT-qPCR and western blot in MDPL HDFs at passages p13 and p20. These analyses aimed to assess the potential influence of in vitro passage-induced aging on POLD1/p125 expression. As shown in Fig. 3, the analyses, evaluated by comparison with age-matched wild-type controls (WT1 and WT2), demonstrated that at p13 *POLD1* mRNA levels were significantly increased in patient BRY ($^{*}p < 0.05$), while remaining unchanged in the older patients PX and LRX. Later, at p20, *POLD1* transcript levels are strongly increased in all patients ($^{****}p < 0.0001$,$^{**}p < 0.01$). (Fig. 3A). By analysing protein expression thought Western blot (WB), we detected a

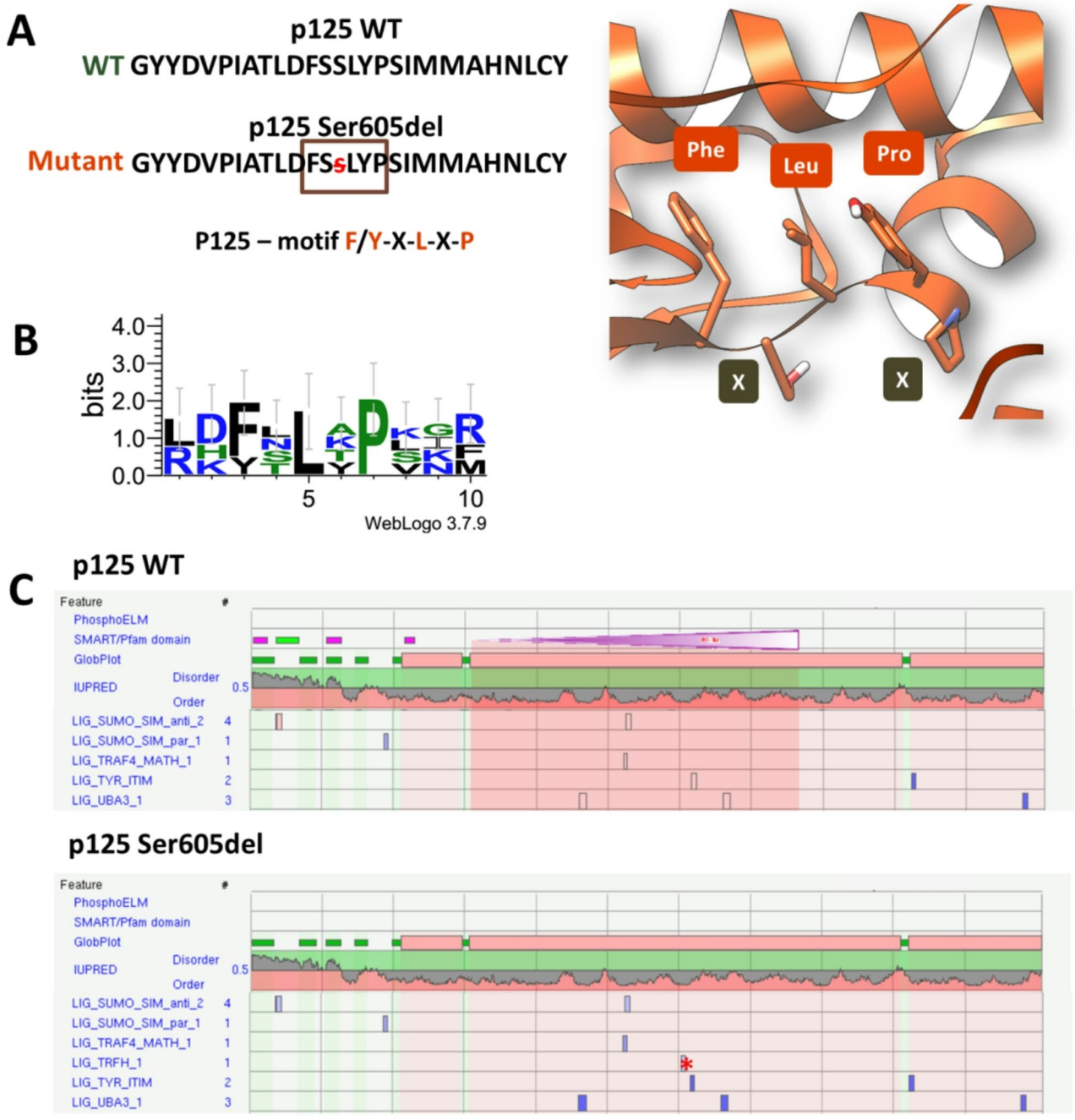

Fig. 2 Gain of a Short Linear Motif for TRF1 Interaction in p125 Ser605del. **A** Sequence alignment of the wild-type (WT) and Ser605del mutant forms of p125. The deletion of Ser605 (highlighted in red) exposes a new F/Y-X-L-X-P motif (in red). Right: cartoon representation of the p125 mutant, showing key conserved residues (Phe, Leu, Pro). **B** Sequence logo illustrating conservation of amino acids within known TRFH-binding motifs, emphasizing the importance of Phe/Tyr, Leu, and Pro residues. **C** Analysis of eukaryotic linear motifs in p125 protein (top) and Ser605del mutant (bottom) using ELM and PROSITE. In the mutant, a putative LIG_TRF1_1 motif (red asterisk) is newly exposed, suggesting a potential gain of interaction with TRF1

strong statistically significant reduction of POLD1 protein level in PX and LRX patients both at p13 and p20, as underlined by densitometric analysis (****$p < 0.0001$, ***$p < 0.001$, **$p < 0.01$) (Fig. 3B). The youngest patient i.e. BRY showed unchanged levels respect to WT1 at both passages.

Indeed, motif analysis identified the acquisition of the linear motif, which is absent in the WT one (Fig. 2A). The identification of LIG_TRFH_1 motif, in Ser605del p125/POLD1 known to mediate interactions with the TRFH domain of TRF1 prompted us to also study its basal

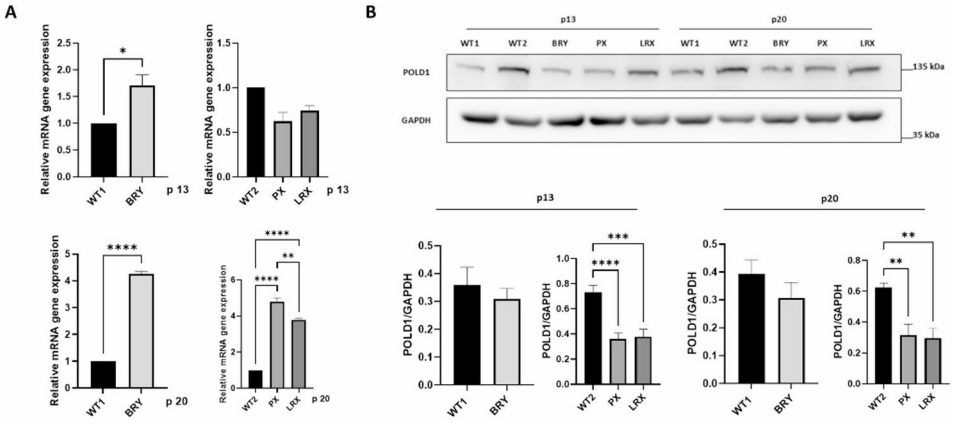

Fig. 3 *POLD1* gene and its protein expression levels. **A** mRNA expression in HDFs was quantified by RT–qPCR using WT as unit at p13 and p20. GAPDH was used as reference gene. **B** Protein extracts were analyzed by western blot; p125/POLD1 levels were normalized on GAPDH. Data are representative of three independent experiments and reported as mean ± SEM. Mean values were compared using the two-tailed Student t-test, for independent samples and One way anova. (p-value *$p < 0.05$, **$p < 0.01$, ***$p < 0.001$, ****$p < 0.0001$)

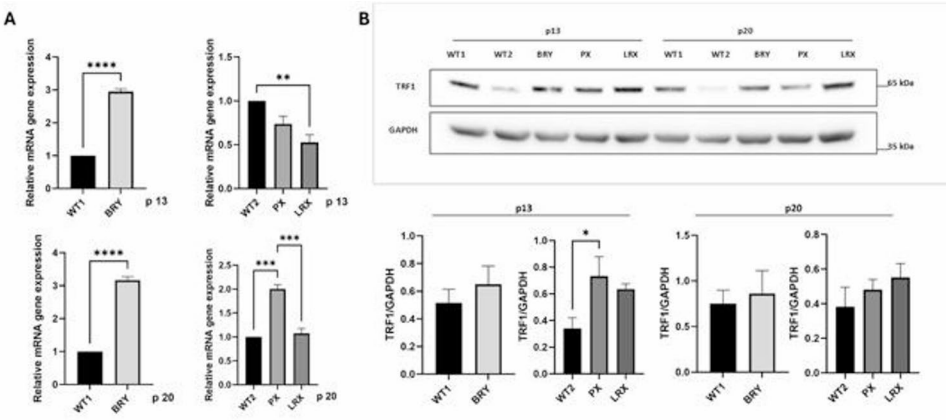

Fig. 4 *TRF1* gene and its protein expression levels. **A** mRNA expression in HDFs was quantified by RT–qPCR using WT as unit at p13 and p20. GAPDH was used as reference gene. **B** Protein extracts were analyzed by western blot; TRF1 levels were normalized on GAPDH. Data are representative of three independent experiments and reported as mean ± SEM. Mean values were compared using the two-tailed Student t-test, for independent samples and One way anova (p-value **$p < 0.01$, ***$p < 0.001$, ****$p < 0.0001$)

expression. TRF1, a member of shelterin complex was investigated at transcript and protein level.

At p13, mRNA expression was heterogeneous among patients, with a strong upregulation in the youngest patient (****$p < 0.0001$) and a tendency to decrease in older patients, statistically significant in LRX (**$p < 0.01$). At late passage, a statistically significant upregulation of TRF1 mRNA transcript levels was evident in all three patients (****$p < 0.0001$, ***$p < 0.001$) (Fig. 4A). Densitometric analysis of WB revealed a clear trend of increased protein levels, which was particularly evident and statistically significant only at p13 for PX (Fig. 4B; *$p < 0.05$).

Role of POLD1 in telomere maintenance: interactions with TRF1

To validate the predictions obtained from eukaryotic linear motifs, we performed an immunoprecipitation assay on POLD1/p125 and confirmed its interaction with TRF1. Notably, this interaction was observed in both MDPL patient (i.e. LRX) and age-matched control (WT 2) (Fig. 5A). Then, we performed a densitometric analysis in which the amount of the TRF1 protein was normalized over the amount of the bait protein immunoprecipitated, p125 (Fig. 5A). By this method, we interestingly demonstrated a higher affinity of TRF1 to the Ser605del p125 compared to the WT (*$p < 0.05$). This finding reveals a previously undescribed potential implication of POLD1/p125 in telomere length regulation. To better validate this data, we immunoprecipitated TRF1, confirming the interaction with POLD1/p125, which was further found to be stronger in MDPL (Fig. 5B).

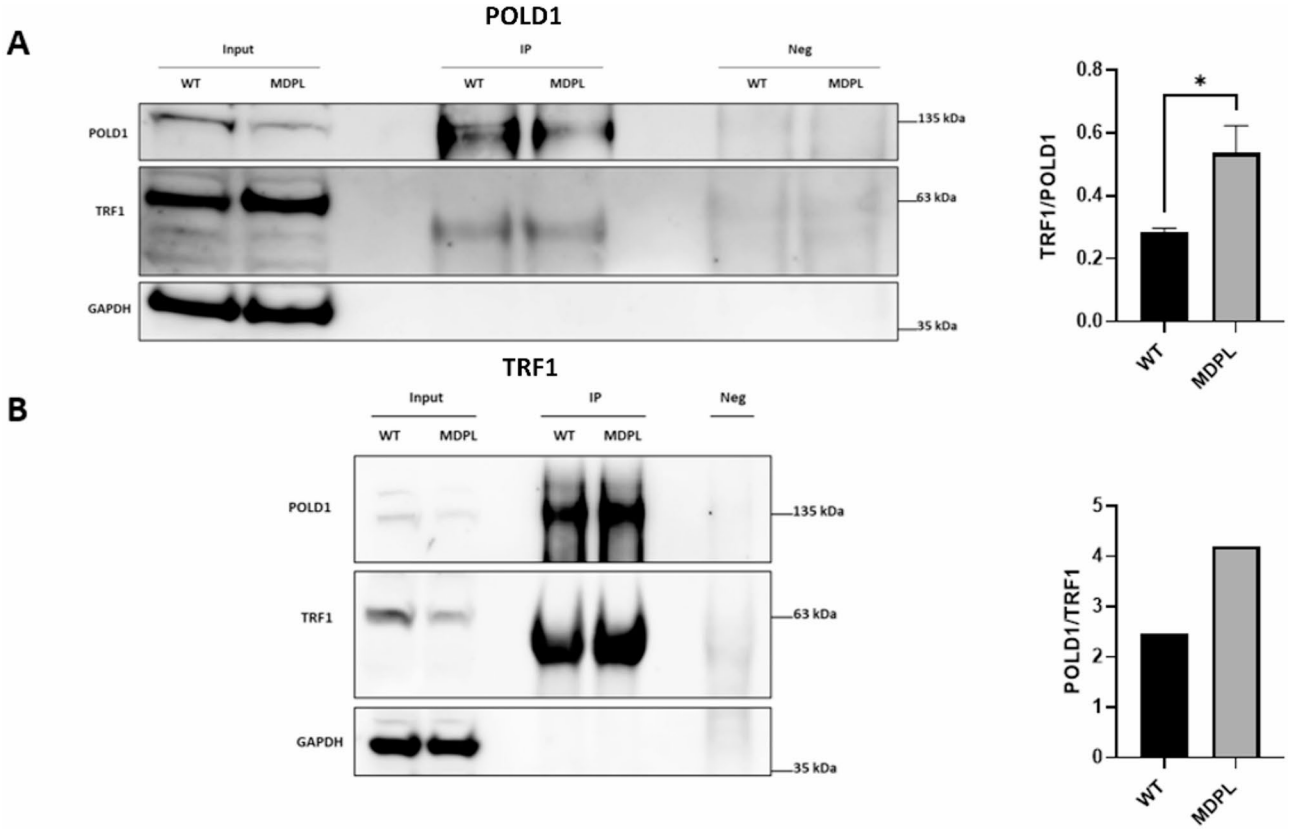

Fig. 5 POLD1/p125-TRF1 interaction. **A** A representative image of POLD1/p125 immunoprecipitated using an anti-POLD1 antibody from whole protein extracts of MDPL and WT HDFs. The predicted interaction with TRF1 was confirmed by western blot, and densitometric analysis was performed by normalizing TRF1 signal to the amount of POLD1/p125. Neg: normal rabbit IgG (Santa Cruz, sc-2027). Data are representative of three independent experiments and reported as mean ± SEM. Mean values were compared using the two-tailed Student t-test (p-value $*p < 0.05$). **B** TRF1 was immunoprecipitated from whole protein extracts of MDPL and WT HDFs. The predicted interaction with POLD1 was confirmed by western blot, and densitometric analysis was performed by normalizing POLD1 signal to the amount of TRF1. Neg: normal rabbit IgG (Santa Cruz, sc-2027)

Structural implications of acquired interaction motifs between p125 and TRF1

To better characterize the mutated p125 pocket, we performed a MDs for WT and mutant protein. To capture the conformational variability of the resulting complexes, we clustered the MD trajectories, obtaining a maximum of five representative structures for each complex. Notably, the F/Y-X-L-X-P motif in p125 is located between two α-helices: L656–L674 and V768–V782. Therefore, we calculated the distances between these helices and the cavity volume of each pocket.

As result, the binding pocket volume was significantly increased in the mutant (429.09 $Å^3$) compared to the WT (164.30 $Å^3$). While the distance between L656 and V782 remains similar in both structures, the mutant exhibits a greater opening between Leu674 and Val768 (29.58 Å) compared to the WT, where the residues are 22.30 Å apart (Fig. 6A).

At this stage, the PPI between the TRFH domain of TRF1 and Ser605del p125 was investigated, in comparison to the WT structure, performing a knowledge-based protein-protein docking, employing HADDOCK 2.4 web-server [18]. Unfortunately, the complete structure of TRF1 has not yet been resolved. Here, we used the TRFH domain of TRF1 from the structure with PDB ID 3BQO, [19] complexed with the TIN2 peptide. After the validation of the docking protocol, we performed docking simulations for TRFH/WT and TRFH/mutant against p125 protein. All the generated complexes were clustered according to their HADDOCK score, calculated as a weighted sum of a variety of energy terms (including van der Waals, electrostatic, desolvation, and restraint violation energies) and buried surface area; Z-score value was also calculated to select the best cluster concerning all obtained clusters: the most negative Z-score is indicative of the top ranked cluster. For the TRF1/$p125_{WT}$ and TRF1/$p125_{Mutant}$ complexes, we obtained 148 structures gathered in 8 clusters, and 143 structures in 9 clusters, respectively. For both complexes, the docking results of the best clusters (the lowest in energy) were reported in Table 1.

It was observed that TRF1/$p125_{Mutant}$ complex showed a stronger theoretical binding affinity with respect to that

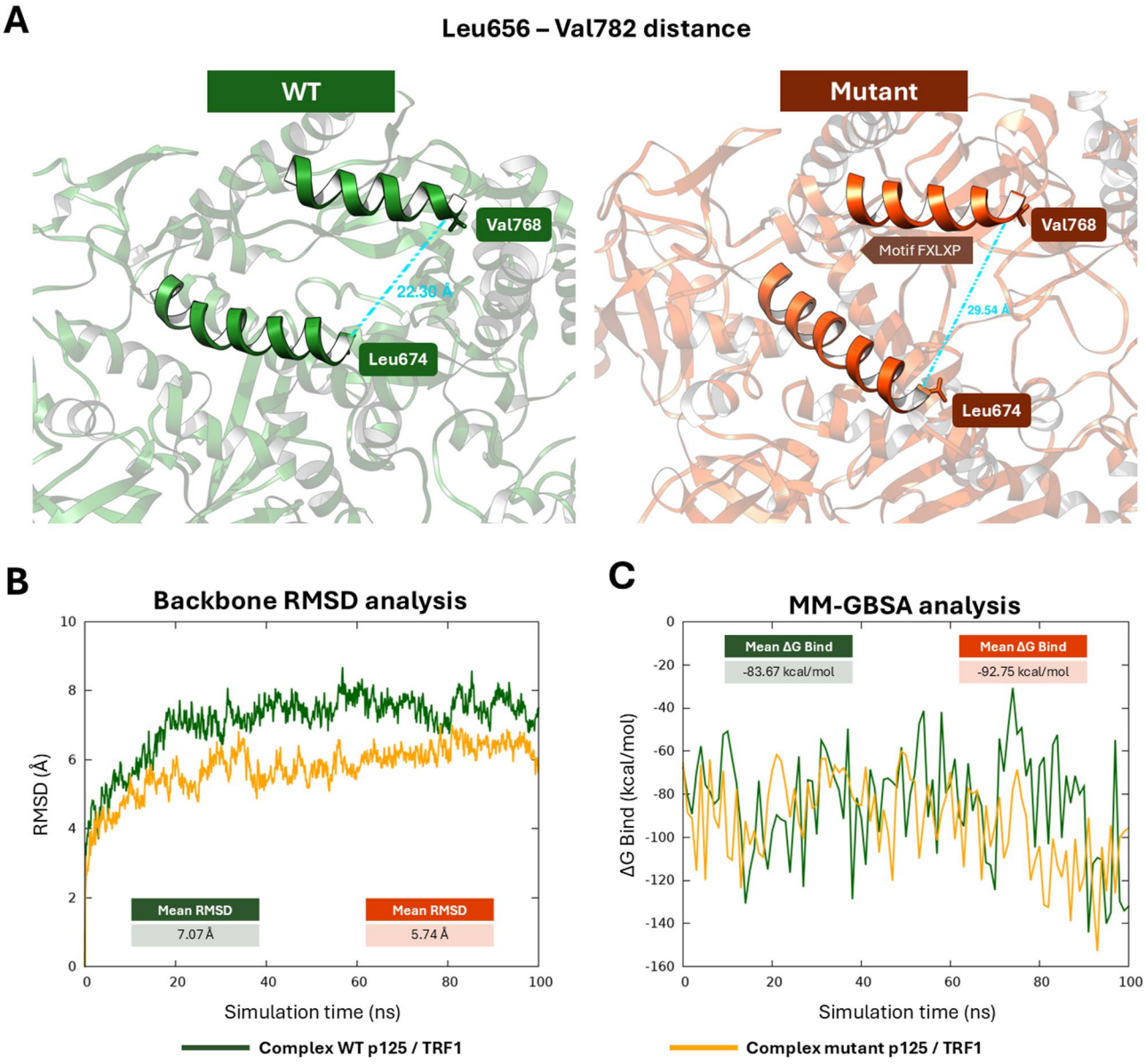

Fig. 6 Comparative Structural and Binding Energy Analysis of TRF1 in complex to WT and Mutant p125. **A** Distance between Leu674 and Val768 in the most representative structures of p125 WT (green) and p125 mutant (orange); **B** Root Mean Square Deviation (RMSD) analysis of the TRF1/$p125_{WT}$ and TRF1/$p125_{Mutant}$ complexes; **C** MM-GBSA binding free energy analysis of TRF1 in complex with WT and mutant p125

Table 1 HADDOCK score values and the associated energetic contributions, expressed in kcal/mol, including Van der Waals, electrostatic, and desolvation energies, for the Docking simulations of TRF1/$p125_{WT}$ and TRF1/$p125_{Mutant}$ complexes

	HADDOCK score*	Van der Waals (kcal/mol)	Electrostatic (kcal/mol)	Desolvatation (kcal/mol)
TRF1/$p125_{WT}$	-94.4 ± 9.0	-28.2 ± 7.0	-389.9 ± 23.4	3.0 ± 3.0
TRF1/$p125_{Mutant}$	-107.9 ± 7.1	-51.8 ± 4.6	-320.6 ± 45.2	2.0 ± 1.9

*The HADDOCK score is defined as: 1.0 Evdw + 0.2 Eelec + 1.0 Edesol + 0.1 EAIR

of TRF1/$p125_{WT}$. The best obtained docked structures for each complex were refined using Protein Preparation Wizard and energy minimized with OPLS_2005 force field.

In order to explore the interaction between TRF1 and p125, we submitted 100 ns of MDs for both complexes. The stability of MDs trajectories was monitored by the RMSD trend of the protein's backbone atoms from its initial conformation. As results, the RMSD trend highlighted that TRF1/$p125_{Mutant}$ was more stable with respect to TRF1/$p125_{WT}$, and the average RMSD values were 7.07 Å and 5.74 Å, for TRF1/$p125_{WT}$ and TRF1/$p125_{Mutant}$ complexes, respectively (Fig. 6B). Additionally,

for both protein–protein complexes, 100 frames extracted by MDs were adopted to calculate the relative binding free energy (ΔG_{bind}) using Molecular Mechanics/Generalized Born Surface Area (MM/GBSA) methodology. As result, MM-GBSA free energy analysis revealed that the TRF1/$p125_{Mutant}$ complex was more favourable than the TRF1/$p125_{WT}$ complex, exhibiting average ΔG_{bind} values of -92.75 kcal/mol and − 83.67 kcal/mol, respectively, thus resulting in a more stabilizing effect of the mutant toward TRF1 recognition. (Fig. 6C).

To better characterize the PPI between p125 and TRF1, a deeper analysis using GBPM was performed on all frames of MDs for each system. This method helps to map the key hotspots responsible for PPI by combining GRID molecular interaction fields (MIFs), according to the GRAB tool algorithm [21]. We considered both $p125_{WT}$ and $p125_{Mutant}$ as hosts and TRF1 as guest. Three GRID probes, such as DRY, N1, and O, were chosen to mimic the hydrophobic, H-bond donor, and acceptor areas, respectively. Considering an energy threshold above the 30% from the global energy minimum GRID points, we summarized the pivotal residues up to 3 Å from GBPM points. The contribution of each residue was derived by the summa of its GBPM points energy in the matching frames. We assessed the contribution of each residue to the PPI by calculating the average percentage of simulation frames in which the residue was involved (Table 2). To enhance clarity, key interaction hotspots were classified into quartiles: Quartile 1 (Q1) comprises residues with the highest frequency, while Quartile 4 (Q4) includes those with the weakest occupancy observed throughout the simulation trajectories.

As shown in the Table 2, the residues of p125 that interact with TRF1 are listed for both the WT and the mutant forms. From this analysis, it is evident that the mutant p125 displays a higher number of interacting residues compared to the WT. Although the total number of residues involved in the interaction is approximately comparable between the two forms, the mutant exhibits a greater number of statistically significant interactions. Specifically, six residues in the mutant p125 interact with TRF1 for more than 15% of the simulation time. Notably, seven of these residues fall within the first (Q1) and second (Q2) quartiles, indicating their consistent and potentially meaningful involvement in the interaction.

Table 2 GBPM average percentage of interactions of the pivotal hotspots of the TRF1/$p125_{WT}$ and TRF1/$p125_{Mutant}$ in complex with TRF1, for all frames of MDs

TRF1/$p125_{WT}$			TRF1/$p125_{Mutant}$		
Residue	**Quartile**	**%**	**Residue**	**Quartile**	**%**
Glu634	Q1	66.4	Asp635	Q1	62.2
Asp635	Q1	60.4	Arg639	Q1	52.9
Lys668	Q2	14.4	Lys648	Q1	34.7
Lys648	Q2	5.9	Arg669	Q2	29.5
Arg791	Q3	1.8	Arg725	Q2	20.0
Lys738	Q3	1.0	Glu634	Q2	19.8
Lys750	Q3	0.6	Lys668	Q2	5.3
His785	Q3	0.6	Arg791	Q3	1.5
Trp781	Q4	0.2	Lys738	Q3	1.4
Lys730	Q4	0.1	Glu301	Q4	0.2
Lys653	Q4	0.1	Lys730	Q4	0.1
Lys732	Q4	0.1			

Investigating potential involvement of PARP1 in MDPL pathogenesis

Due to the correlation between TRF1 and PARP1 and to PARP1 involvement in many important DNA repair mechanisms and in aging regulation [24, 25, 26], we evaluated its transcript expression in MDPL HDFs at passages 13 and 20 (Fig. 7A). The analysis revealed a strong downregulation of *PARP1* transcript levels in PX and LRX at both p13 and p20 respect to WT age-matched (****$p < 0.,0001$, ***$p < 0.001$, **$p < 0.01$), while in BRY, its expression remained unchanged.

Protein expression (Fig. 7B) mirrored the transcriptional trend: while in the two older patients (PX and LRX) the downregulation of this marker was confirmed compared to age-matched controls (***$p < 0.001$, **$p < 0.01$) in BRY, PARP1 protein levels remained unchanged at both p13 and p20.

These findings provide a starting point for further investigation into the potential role indirectly played by PARP1 into MDPL pathogenesis.

Protein expression in X-rays irradiated HDFs

Considering the role of POLD1/p125 in DNA repair mechanisms and our previous data regarding MDPL defect in DNA damage response process [10], we repeated the above experiments in the presence of DNA damage induction. Therefore, for an accurate assessment of the impact of the Ser605del variant on POLD1, HDFs were exposed to X-rays at an intensity of 1 Gy and the analyses have been performed after 24 h during the DNA repair kinetics, as previously reported by us on MDPL HDFs cells [10]. In this way, data were analyzed by comparing irradiated MDPL HDFs (IRR) to their respective baseline condition (CTR: unirradiated MDPL) for each patient at evaluating the expression of the three pivotal proteins: POLD1, TRF1 and PARP1(Fig. 8A).

A decreasing trend was observed for POLD1 protein in presence of DNA damage at p13, statistically significant both for PX and BRY, (**$p < 0.001$, *$p < 0.05$) (Fig. 8B). Notably, TRF1 also decreased after DNA damage at p13 (statistically significant for PX, *$p < 0.05$), while it remains unchanged in the younger patient BRY (Fig. 8C). Finally, PARP1 expression manifests a decreasing trend at p13, statistically significant only for PX14 (*$p < 0.05$) (Fig. 8D).

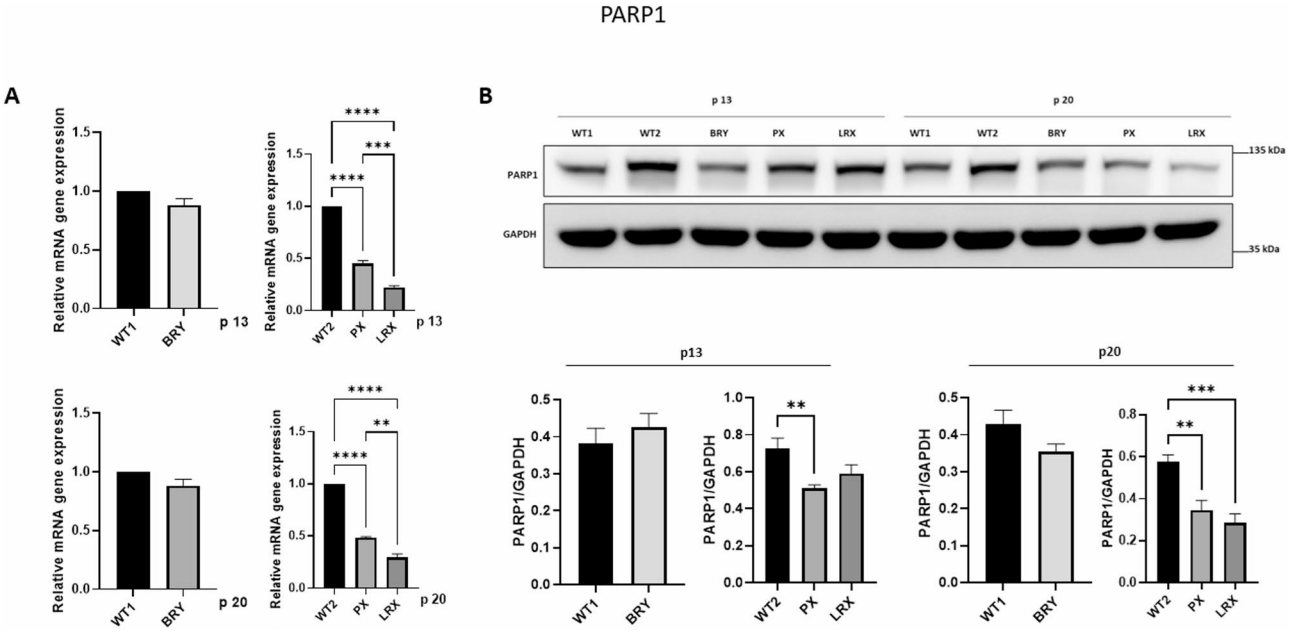

Fig. 7 *PARP1* gene and its protein expression levels. **A** mRNA expression in HDFs was quantified by RT–qPCR using WT as unit at p13 and p20. GAPDH was used as reference gene. **B** Protein extracts were analyzed by western blot; PARP1 levels were normalized on GAPDH. Data are representative of three independent experiments and reported as mean ± SEM. Mean values were compared using the two-tailed Student t-test, for independent samples and One way anova. (p-value $^{**}p < 0.01$, $^{***}p < 0.001$, $^{****}p < 0.0001$)

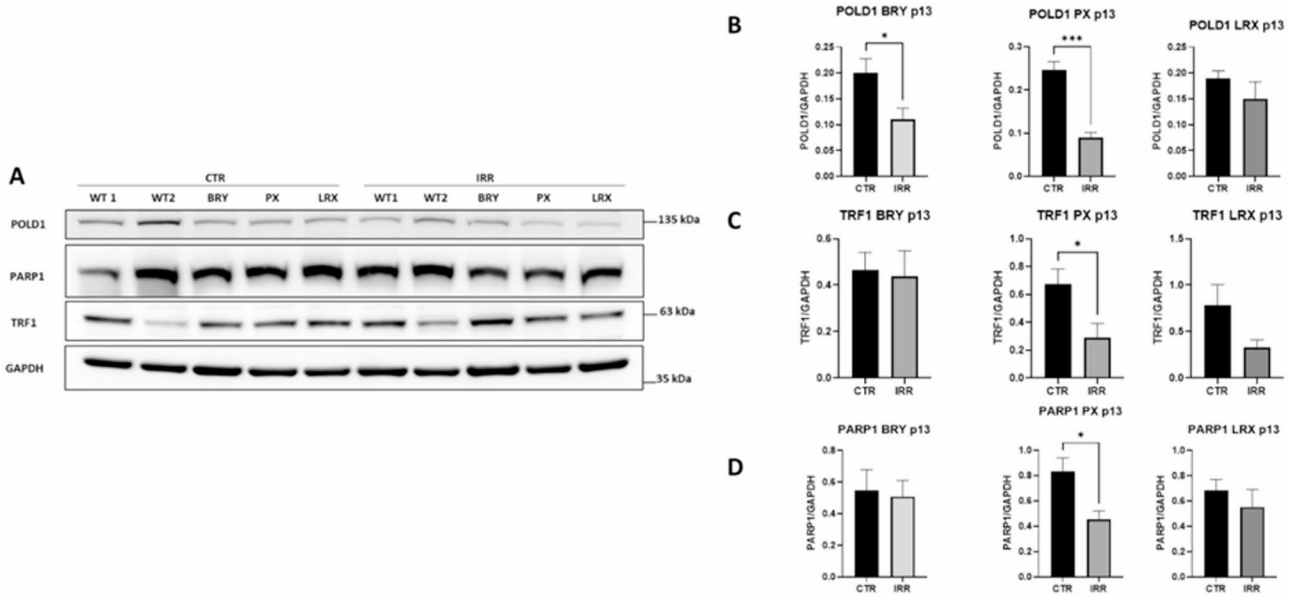

Fig. 8 Evaluation of protein expression levels after 24 h X-ray irradiation in MDPL HDFs (IRR)compared to the same not irradiated ones (CTR) at p13. **A** Representative western blot image. **B** POLD1/p125 densitometric analysis comparing MDPL HDFs after 1 Gy X-irradiation (IRR) to not irradiated ones (CTR). **C** TRF1 densitometric analysis comparing MDPL HDFs after 1 Gy X-irradiation (IRR) to not irradiated ones (CTR). **D** PARP1 densitometric analysis comparing MDPL HDFs after 1 Gy X-irradiation (IRR) to not irradiated ones (CTR). Data are representative of three independent experiments and reported as mean ± sem. Mean values were compared using the two-tailed student t-test, for independent samples (p-value $^{*}p < 0.05$, $^{***}p < 0.001$)

Finally, we aimed to investigate whether the previously described interaction between p125/POLD1and TRF1 was dependent on the induction of DNA damage, particularly regarding changes in the affinity of these proteins involved in DNA repair kinetics. To evaluate this, we performed immunoprecipitation of p125/POLD1 after 1 Gy irradiation, and the interaction was analysed by immunoprecipitation 24 h later, as standardized in our previous experiments [10].Under these conditions, we were unable to observe any difference in the amount

of TRF1 bound to POLD1 HDFs in MDPL compared to WT ones (data not shown).

Discussion

Mandibular Hypoplasia, Deafness, Progeroid Features, and Lipodystrophy (MDPL) is an autosomal dominant disorder characterised by a constellation of clinical features including prominent loss of subcutaneous fat, distinctive facial traits, and sensorineural deafness [27]. As of 2024, fewer than 40 cases have been reported worldwide, underscoring its rarity. Most patients carry a recurrent frame deletion (p. Ser605del) within the polymerase active site, in the catalytic subunit p125 of POLD1. The deletion severely compromises enzyme's catalytic activity while only partially affecting its proofreading capabilities [8]. Functional analyses have shown that Ser605del variant results in a complete loss of polymerase activity, although exonuclease activity is preserved to a certain extent. This decoupling of enzymatic activities likely leads to increased genomic instability and probably contributes to the clinical manifestations of the Syndrome through a still unresolved mechanism.

In silico approaches, such as docking simulations, MD simulations and MMGB/SA analyses, helped to indeep investigate how the mutation compromises protein activity. Structurally, the loss of Ser605 perturbs the local H-bond network, leading to increased conformational fluctuations that may affect substrate positioning. Such instability could compromise the enzyme's ability to maintain an optimal active site geometry, reducing polymerization efficiency. From a thermodynamic perspective, reduced binding affinity could led to an unfavorable energetic environment for nucleotide incorporation in Ser605del p125 structure. A reduced capacity to retain the substrate may directly impact POLD1's function, highlighting the potential consequences of this mutation in disease-related contexts.

To investigate the impact of the deletion on protein-protein interactions, we analyzed SLiMs using the ELM and PROSITE databases in both WT and Ser605del p125. The ELM analysis predicted potential changes in motif acquisition due to the mutation, suggesting altered binding affinities and interaction profiles. Specifically, the mutant form gained the interesting LIG_TRFH_1 motif, which is not present in the WT protein. Specifically, the deletion of Ser605 generates a new linear motif (FSLYP) that aligns with the F/Y-X-L-X-P consensus of the LIG_TRFH_1 motif, known to mediate interactions with the TRFH domain of TRF1. This suggests that the mutation is not merely neutral or a loss-of-function but may actually lead to the acquisition of a novel binding capability. Indeed, the combined use of a sequence logo, which shows that the FSLYP motif conforms to key positions within the TRFH-binding consensus, and bioinformatics analysis, which explicitly identify the LIG_TRFH_1 motif only in the mutant and not in the wild-type protein, provides strong predictive support that the mutation induces non-trivial structural and functional changes. Crystallographic studies from literature have demonstrated that the F/Y-X-L-X-P motif plays a crucial role in mediating interactions between various proteins and the TRFH domains of TRF1. With purpose, TRF1 is a marker strikingly correlated to MDPL disease because it plays a crucial role in preserving telomere integrity by supporting DNA replication and preventing damage caused by subtelomeric recombination. It is also essential in safeguarding critically short telomeres from aberrant recombination events, thereby maintaining telomere stability [9, 11]. Structurally, TRF1 consists of the TRFH domain, which mediates interactions with various shelterin-associated proteins, a central domain, and Myb domains. These bind directly to the minor groove of DNA, conferring high binding affinity to telomeric double-stranded DNA (dsDNA) regions. The TRFH domain is an evolutionarily conserved PPI region that often utilizes a concave groove to bind a short motif in its interacting proteins. Thus, the conserved sequence F/Y-X-L-X-P, found in p125, could represent the putative motif to recognize the TRFH domain.

Based on this newly formulated hypothesis of an acquired interaction, we first investigated in silico the potential binding affinity between TRF1 and both the WT and mutant forms of p125.

Cavity volume analysis revealed that the F/Y-X-L-X-P motif became more exposed due to the increased opening of two helices in the Ser605del p125. This conformational change could facilitate a more effective interaction with TRF1. Indeed, in silico analysis revealed a higher binding affinity between TRF1 and the mutant form of p125 compared to the WT one, as evidenced by more favorable energy interaction values. Moreover, although the total number of residues involved in the interaction is similar between the WT and mutant forms of p125, the mutant form exhibits a greater number of statistically significant interactions with TRF1. This suggests that the mutation does not simply alter the binding surface, but rather optimizes the interaction in a way that makes it more stable and functionally relevant.

All these preliminary observations lay a solid foundation for experimental validation. Thus, we first analysed the transcript and protein expression levels of POLD1 and TRF1 in patients and age-matched WT individuals, to capture the basal state of these two involved markers. *POLD1* mRNA levels are significantly increased only in the youngest patient at passage 13, while at late passage, *POLD1* transcript levels are strongly increased in all patients. Conversely, by analysing protein expression, we detected a strong and statistically significant reduction

in the adult patients at both p13 and p20. These results demonstrate the effect of the Ser605del mutation on protein expression levels in an age-dependent manner. From this perspective, the upregulation of gene expression of *POLD1* could be explained as a compensatory mechanism activated by MDPL cells.

At this regard, our results revealed that Ser605del destabilizes the p125 structure, thus we hypothesize that this could influence the activity and stabilization of the Polδ complex, thereby activating degradation mechanisms.

Regarding TRF1, mRNA expression was heterogeneous among patients, but a clear trend of increased protein levels was observed. Interestingly, overexpression of TRF1 has been previously described in HTC75, a telomerase-positive fibrosarcoma cell line commonly used in telomere research, and it is associated with a gradual decline in telomere length, a phenomenon we have already observed in MDPL HDFs [28].

Immunoprecipitation assays, performed for the first time in this context, confirmed the interaction between p125/POLD1 and TRF1. This interaction was experimentally detected in both MDPL patients and healthy controls. Notably, it had never been investigated before, not even in wild-type models. Most significantly, the Ser605del p125 mutant protein showed a stronger binding affinity for TRF1 compared to the wild-type protein, consistent with predictions from in silico simulations. TRF1 binds telomeric DNA via its Myb domain, while its TRFH domain mediates protein-protein interactions. Binding of POLD1 to the TRFH domain could potentially hinder TRF1's access to telomeric DNA due to the large size of POLD1 or the full Pol δ complex. Additional experiments will be needed to validate this hypothesis. .

Considering the novel link between TRF1 and POLD1/P125 in MDPL syndrome, we also investigated the possible involvement of PARP1 in the molecular landscape of the disease, prompted by a recent study of Maresca and collaborators describing how poly(ADP-ribose) polymerase 1 (PARP1) interacts with and covalently PARylates TRF1 during S-phase, thereby modulating its DNA-binding affinity [27, 28]. PARP1 has been widely implicated in aging-related processes and is considered an antagonistic pleiotropic factor: protective in early life but potentially detrimental in aging or under stress.

PARP1, a key member of the human poly (ADP-ribose) polymerase family, plays a central role in chromatin remodeling, cell cycle regulation, DNA replication, and multiple DNA repair pathways, thus acting as a general caretaker of genomic stability [25, 30]. Consistently, PARP1−/− mice and derived cells exhibit hypersensitivity to DNA-damaging agents and elevated genomic instability [24]. In addition, PARP1 knockout is associated with a premature aging phenotype [31]. Although its precise role in telomere regulation remains debated, whether promoting shortening or lengthening, PARP1 clearly influences telomere dynamics. On one hand, it preserves cellular function under normal conditions; on the other, it may contribute to functional decline and cell death under pathological or aged conditions [25].

Our analysis of *PARP1* mRNA and protein expression in MDPL cells revealed a strong downregulation in adult patients at both p13 and p20 compared to age-matched controls, whereas expression remained unchanged in the youngest patient. The marked downregulation of both PARP1 transcript and protein levels aligns with the known hallmarks of aging observed in MDPL HDF.

In summary, the transcript and protein expression levels of *POLD1*, *TRF1* and *PARP1*, revealed a common trend in the older patients (PX and LRX). All these data allowed us to speculate that PARP1 could also be involved into pathogenetic mechanism of MDPL Syndrome, although further experiments will be necessary to clarify its role in the disease.

In our previous work, we deepen MDPL HDFs patients after damage induction by X-ray in order to exacerbate the cellular phenotype. The evaluation of genomic instability revealed a delayed recovery from DNA damage. Furthermore, the rate of telomere shortening was higher in pathological cells, indicating telomere dysfunction as an emerging hallmark of MDPL.

These findings suggested that an altered DNA replication and repair function of POLD1 may represent a primary pathogenic mechanism in MDPL. X-ray irradiation (1 Gy) was used to study DNA repair kinetics independently from damage induction. MDPL-HDFs showed defective repair specifically in the HR phase, particularly at telomeres, where NHEJ is inhibited. This defect led to increased telomeric damage and failure to resolve it efficiently, as shown by TIF analysis. The persistent activation of Polδ and the faster telomere shortening observed in MDPL cells suggest that impaired HR at telomeres contributes to their premature senescence [10]. Considering the role of POLD1 in DNA repair mechanisms and the previously observed defects in MDPL regarding DNA damage response, we reevaluated the expression of POLD1, TRF1 and PARP1 proteins in MDPL patients after damage induction by X-ray, as previously described [10]. These results indicated a generalized reduction in protein expression (not always statistically significant), suggesting negative regulation after DNA damage induction in MDPL patients. Interestingly, previous studies in yeast have revealed proteasomal degradation of the catalytic subunit of the DNA polymerase δ following UV irradiation [32]. These data further suggest that there is a link between these three proteins underlying the disease. Of course, further research is essential to support our hypothesis. The fact remains that in this study we have

demonstrated for the first time the involvement of TRF1, which directly binds to POLD1 protein.

Our results provide new information that has never been described before on the Ser605del variant within the polymerase active site, in the catalytic subunit p125 of POLD1. Our study suggest that the Ser605del not only destabilizes the substrate binding but also induces conformational changes that compromise the overall structural integrity of POLD1. This instability may underlie the reduced processivity observed experimentally in the mutant POLD1, highlighting the crucial role of Ser605del in ensuring efficient DNA synthesis.

POLD1 in presence of deletion in Ser605 leads to the acquisition of a telomere-specific interaction motif and the retention of phosphorylation motifs, emphasizing the mutation's potential influence on telomere biology and protein function.

Furthermore, Ser605del perturbs *POLD1* mRNA and protein expressions levels in an age-dependent manner, as previously described by us in mesenchymal stem cells [32]. However, the higher affinity of Ser605del POLD1 to TRF1, associated with the reduction of PARP1, responsible for regulation the affinity between TRF1 and telomeres, enhances the landscape of premature aging phenomena observed in MDPL patients. These results could allow us to speculate onthe existence of a dual telomere surveillance mechanism, mediated by POLD1 and PARP1,that appears to be impaired in MDPL syndrome. Future experiments will clarify the molecular mechanisms underlying this regulation.

Limitations of the study

This study provides important structural insights into the impact of the Ser605del mutation in POLD1 and its potential role in modulating interactions with TRF1 and downstream pathways involving PARP1. However, several limitations should be acknowledged. First, given the extremely rare nature of the genetic disorder (40 patients reported worldwide), increasing the number of patients would strengthen the validity of our findings. Also, no quantitative differences in POLD1/TRF1 immunoprecipitation were detected after X-ray irradiation between wild type and MDPL cells. This observation may suggest that alternative forms of DNA damage, such as hydrogen peroxide or UV exposure, may be required to better elucidate the interaction between these two key aging-related markers. Even if reduced levels of PARP1 transcript and protein were detected, the involvement of PARP1 into the pathogenetic mechanism of the disease remains to be further elucidated, beyond the structural level. Indeed, there is solid biological evidence supporting the interaction between PARP1 and TRF1, particularly in the context of the cellular response to replicative stress, where PARP1 can modify TRF1, influencing its binding dynamics to telomeric DNA and contributing to telomere stability. However, no high-resolution structural models (such as crystallography or cryo-EM) describing this interaction in detail are currently available. This represents an important limitation in studying the POLD1–TRF1–PARP1 axis, as the observed links among these proteins may be indirect or mediated by other factors, such as cofactors, enzymatic modifications, or complex nucleoprotein structures. To fill this gap, obtaining the complete high-resolution structures of TRF1 and PARP1, as well as their complexes, will be essential to clarify their direct interactions and regulatory mechanisms.

Supplementary Information

The online version contains supplementary material available at https://doi.org/10.1186/s40246-025-00848-0.

Supplementary Material 1.

Acknowledgements

This research was supported by Italian MUR PRIN– Prot. 20223WFJJ3.

Author contributions

Conceptualization, M.M. and I.R.; methodology, I.R., M.M., S.M., A.C.G.P; Investigation, I.R., M.M., S.M., A.C., G.P., writing—original draft, M.M. I.R. and S.M. writing—review & editing, F.S.,G.N.,M.H.C.,S.A funding acquisition F.S; supervision, G.N and S.A.

Data availability

Data is provided within the manuscript or supplementary information files.

Declarations

Competing interests

The authors declare no competing interests.

Author details

[1]Department of Biomedicine and Prevention, University of Rome Tor Vergata, Via Montpellier 1, Rome 00133, Italy
[2]Dipartimento di Scienze della Salute, Università "Magna Graecia" di Catanzaro, Campus "S. Venuta", Viale Europa, Catanzaro 88100, Italy
[3]Net4Science S.r.l. Academic Spin-Off, Università "Magna Graecia" di Catanzaro, Campus "S. Venuta", Viale Europa, Catanzaro 88100, Italy
[4]Department of Biology, University of Rome "Tor Vergata", via della Ricerca Scientifica 1, Rome 00133, Italy

Received: 20 August 2025 / Accepted: 9 October 2025
Published online: 12 November 2025

References

1. Cheng F, Zhao J, Wang Y, Lu W, Liu Z, Zhou Y, Martin WR, Wang R, Huang J, Hao T. Comprehensive characterization of protein–protein interactions perturbed by disease mutations. Nat Genet. 2021;53(3):342–53.
2. Nichols-Vinueza DX, Delmonte OM, Bundy V, Bosticardo M, Zimmermann MT, Dsouza NR, Pala F, Dobbs K, Stoddard J, Niemela JE. POLD1 deficiency reveals a role for POLD1 in DNA repair and T and B cell development. J Clin Immunol. 2021;41(1):270–3.
3. Xie B, Mazloum N, Liu L, Rahmeh A, Li H, Lee MY. Reconstitution and characterization of the human DNA polymerase delta four-subunit holoenzyme. Biochemistry. 2002;41(44):13133–42.
4. Shin Y, Hedglin M, Murakami KS. Cryo-EM structure of apo-form human DNA polymerase δ elucidates its minimal DNA synthesis activity without PCNA. J Biol Chem. 2025;301(4):108342.

5. Lancey C, Tehseen M, Raducanu V-S, Rashid F, Merino N, Ragan TJ, Savva CG, Zaher MS, Shirbini A, Blanco FJ. Structure of the processive human pol δ holoenzyme. Nat Commun. 2020;11(1):1109.
6. Zhou Y, Meng X, Zhang S, Lee EY, Lee MY. Characterization of human DNA polymerase delta and its subassemblies reconstituted by expression in the multibac system. PLoS ONE 2012;7(6):e39156.
7. Zuo B, Xu H, Pan Z, Mao L, Feng H, Zeng B, Tang W, Lu W. A likely pathogenic POLD1 variant associated with mandibular hypoplasia, deafness, progeroid features, and lipodystrophy syndrome in a Chinese patient. BMC Med Genom. 2022;15(1):220.
8. Weedon MN, Ellard S, Prindle MJ, Caswell R, Allen HL, Oram R, Godbole K, Yajnik CS, Sbraccia P, Novelli G. An in-frame deletion at the polymerase active site of POLD1 causes a multisystem disorder with lipodystrophy. Nat Genet. 2013;45(8):947–50.
9. Azarm K, Bhardwaj A, Kim E, Smith S. Persistent telomere cohesion protects aged cells from premature senescence. Nat Commun. 2020;11(1):3321.
10. Murdocca M, Spitalieri P, De Masi C, Udroiu I, Marinaccio J, Sanchez M, Talarico RV, Fiorillo C, D'Adamo M, Sbraccia P. Functional analysis of POLD1 p. ser605del variant: the aging phenotype of MDPL syndrome is associated with an impaired DNA repair capacity. Aging. 2021;13(4):4926.
11. Wang L, Tu Z, Liu C, Liu H, Kaldis P, Chen Z, Li W. Dual roles of TRF1 in tethering telomeres to the nuclear envelope and protecting them from fusion during meiosis. Cell Death Differ. 2018;25(6):1174–88.
12. Shivakumar D, Harder E, Damm W, Friesner RA, Sherman W. Improving the prediction of absolute solvation free energies using the next generation OPLS force field. J Chem Theory Comput. 2012;8(8):2553–8.
13. Friesner RA, Banks JL, Murphy RB, Halgren TA, Klicic JJ, Mainz DT, Repasky MP, Knoll EH, Shelley M, Perry JK. Glide: a new approach for rapid, accurate Docking and scoring. 1. Method and assessment of Docking accuracy. J Med Chem. 2004;47(7):1739–49.
14. Bowers KJ, Chow E, Xu H, Dror RO, Eastwood MP, Gregersen BA, Klepeis JL, Kolossvary I, Moraes MA, Sacerdoti FD. In *Scalable algorithms for molecular dynamics simulations on commodity clusters*, Proceedings of the. 2006 ACM/IEEE Conference on Supercomputing, 2006; pp 84-es.
15. Jorgensen WL, Chandrasekhar J, Madura JD, Impey RW, Klein ML. Comparison of simple potential functions for simulating liquid water. J Chem Phys. 1983;79(2):926–35.
16. Genheden S, Ryde U. The MM/PBSA and MM/GBSA methods to estimate ligand-binding affinities. Expert Opin Drug Discov. 2015;10(5):449–61.
17. Halgren TA. Identifying and characterizing binding sites and assessing druggability. J Chem Inf Model. 2009;49(2):377–89.
18. Van Zundert G, Rodrigues J, Trellet M, Schmitz C, Kastritis P, Karaca E, Melquiond A, van Dijk M, De Vries S, Bonvin A. The HADDOCK2. 2 web server: user-friendly integrative modeling of biomolecular complexes. J Mol Biol. 2016;428(4):720–5.
19. Chen Y, Yang Y, Van Overbeek M, Donigian JR, Baciu P, de Lange T, Lei M. A shared Docking motif in TRF1 and TRF2 used for differential recruitment of telomeric proteins. Science. 2008;319(5866):1092–6.
20. Pettersen EF, Goddard TD, Huang CC, Couch GS, Greenblatt DM, Meng EC, Ferrin TE. UCSF Chimera—a visualization system for exploratory research and analysis. J Comput Chem. 2004;25(13):1605–12.
21. Ortuso F, Langer T, Alcaro SGBPM. GRID-based pharmacophore model: concept and application studies to protein–protein recognition. Bioinformatics. 2006;22(12):1449–55.
22. Bivacqua R, Romeo I, Barreca M, Barraja P, Alcaro S, Montalbano A. HSV-1 glycoprotein D and its surface receptors: evaluation of Protein–Protein interaction and targeting by Triazole-Based compounds through in Silico approaches. Int J Mol Sci. 2023;24(8):7092.
23. Jumper J, Evans R, Pritzel A, Green T, Figurnov M, Ronneberger O, Tunyasuvunakool K, Bates R, Žídek A, Potapenko A. Highly accurate protein structure prediction with alphafold. Nature. 2021;596(7873):583–9.
24. Mangerich A, Bürkle A. Pleiotropic cellular functions of PARP1 in longevity and aging: genome maintenance Meets inflammation. Oxidative Med Cell Longev. 2012;2012(1):321653.
25. Mao K, Zhang G. The role of PARP1 in neurodegenerative diseases and aging. FEBS J. 2022;289(8):2013–24.
26. Maresca C, Dello Stritto A, D'Angelo C, Petti E, Rizzo A, Vertecchi E, Berardinelli F, Bonanni L, Sgura A,Antoccia A. PARP1 allows proper telomere replication through TRF1 Poly (ADP-ribosyl) ation and helicase recruitment. Commun Biology. 2023;6(1):234.
27. Reinier F, Zoledziewska M, Hanna D, Smith JD, Valentini M, Zara I, Berutti R, Sanna S, Oppo M, Cusano R. Mandibular hypoplasia, deafness, progeroid features and lipodystrophy (MDPL) syndrome in the context of inherited lipodystrophies. Metabolism. 2015;64(11):1530–40.
28. Van Steensel B, De Lange T, Smogorzewska A, van Steensel B, Bianchi A, Oelmann S, Schaefer MR, Schnapp G, de Lange T, editors. Control of telomere length by the human telomeric protein TRF1. *Nature* 1997, *385* (6618), 740–743; (b) Smogorzewska A, van Steensel B, Bianchi A, Oelmann S, Schaefer MR, Schnapp G, de Lange T. Control of human telomere length by TRF1 and TRF2. *Molecular and cellular biology* 2000, *20* (5), 1659–1668.
29. Aguennouz MH, Vita GL, Messina S, Cama A, Lanzano N, Ciranni A, Rodolico C, Di Giorgio RM, Vita G. Telomere shortening is associated to TRF1 and PARP1 overexpression in Duchenne muscular dystrophy. Neurobiol Aging. 2011;32(12):2190–7.
30. Alemasova EE, Lavrik OI. Poly (ADP-ribosyl) ation by PARP1: reaction mechanism and regulatory proteins. Nucleic Acids Res. 2019;47(8):3811–27.
31. Piskunova TS, Yurova MN, Ovsyannikov AI, Semenchenko AV, Zabezhinski MA, Popovich IG, Wang Z-Q, Anisimov VN. Deficiency in Poly (ADP-ribose) Polymerase-1 (PARP-1) accelerates aging and spontaneous carcinogenesis in mice. Curr Gerontol Geriatr Res. 2008;2008(1):754190.
32. Daraba A, Gali VK, Halmai M, Haracska L, Unk I. Def1 promotes the degradation of Pol3 for polymerase exchange to occur during DNA-damage–induced mutagenesis in Saccharomyces cerevisiae. PLoS Biol 2014;12(1):e1001771.

Publisher's note

Springer Nature remains neutral with regard to jurisdictional claims in published maps and institutional affiliations.